Yang, X., **Zhang, X.**, **Graeber, D.**, Hensley, R., Jarvie, H., Lorke, A., **Borchardt, D.**, Li, Q., **Rode, M.** (2023):
Large-stream nitrate retention patterns shift during droughts: seasonal to sub-daily insights from high-frequency data-model fusion
Water Res. **243** , art. 120347

https://doi.org/10.1016/j.watres.2023.120347

Large-stream nitrate retention patterns shift during droughts: seasonal to sub-daily insights from high-frequency data-model fusion

Xiaoqiang Yang[a,b], Xiaolin Zhang[b], Daniel Graeber[b], Robert Hensley[c], Helen Jarvie[d], Andreas Lorke[e], Dietrich Borchardt[b], Qiongfang Li[f,a] and Michael Rode[b,g]

[a]Yangtze Institute for Conservation and Development, Hohai University, Nanjing, 210098, China

[b]Department of Aquatic Ecosystem Analysis and Management, Helmholtz Centre for Environmental Research - UFZ, Magdeburg, 39114, Germany

[c]Battelle - National Ecological Observatory Network, Boulder, 80301, U.S.

[d]Department of Geography and Environmental Management, University of Waterloo, Waterloo, Ontario N2L 3G1, Canada

[e]Institute for Environmental Sciences, University of Koblenz-Landau, Landau, 76829, Germany.

[f]College of Hydrology and Water Resources, Hohai University, Nanjing, 210098, China

[g]Institute of Environmental Science and Geography, University of Potsdam, Potsdam, 14476, Germany

Corresponding author: Xiaoqiang Yang (xiaoqiang.yang@ufz.de)

Abstract

High-frequency nitrate-N ($NO_3^- - N$) data are increasingly available, while accurate assessments of in-stream $NO_3^- - N$ retention in large streams and rivers require a better capture of complex river hydrodynamic conditions. This study demonstrates a fusion framework between high-frequency water quality data and hydrological transport models, that (1) captures river hydraulics and their impacts on solute signal propagation through river hydrodynamic modeling, and (2) infers in-stream retention as the differences between conservatively traced and reactively observed $NO_3^- - N$ signals. Using this framework, continuous 15-min estimates of $NO_3^- - N$ retention were derived in a 6th-order reach of the lower Bode River (27.4 km, central Germany), using long-term sensor monitoring data during a period of normal flow from 2015-2017 and a period of drought from 2018-2020. The unique $NO_3^- - N$ retention estimates, together with metabolic characteristics, revealed insightful seasonal patterns (from high net autotrophic uptake in late-spring to lower uptake, to net heterotrophic release during autumn) and drought-induced variations of those patterns (reduced levels of net uptake and autotrophic nitrate uptake largely buffered by heterotrophic release processes, including organic matter mineralization). Four clusters of diel uptake patterns were identified, potentially representing changes in dominant $NO_3^- - N$ retention processes according to seasonal and hydrological conditions. For example, dominance of autotrophic $NO_3^- - N$ retention extended more widely across seasons during the drought years. Such cross-scale patterns and changes under droughts are likely co-determined by catchment and river environments (e.g., river primary production, dissolved organic carbon availability and its quality), which resulted in more complex responses to the sequential droughts. Inferences derived from this novel data-model fusion provide new insights into NO_3^- dynamics and ecosystem function of large streams, as well as their responses to climate variability. Moreover, this framework can be flexibly transferred across sites and scales, thereby complementing high-frequency monitoring to identify in-stream uptake processes and to inform river management.

Key words: long-term high-frequency monitoring; river hydrodynamic model; conservative tracer simulation; river metabolism; droughts; river ecosystem function

1 Introduction

Anthropogenically induced high nitrate (NO_3^-) levels in rivers are a pervasive threat to freshwater and costal ecosystems, especially under the changing climate (Costa et al., 2022; Reusch et al., 2018; Rockström et al., 2009). In addition to efforts to control point- and diffuse-sources, the “self-cleansing” capacity of river systems to retain and process NO_3^- has also been recognized (Ensign and Doyle, 2006; Jäger et al., 2017). Restoring rivers and their floodplains has been advocated as a part of “natural-based” solutions to reduce NO_3^- losses to water bodies, with multiple co-benefits (EEA, 2021).

Large streams and rivers (e.g., ≥ 4th order) receive considerable management attention, due to the impacts of nutrient pollution on water-related ecosystem services, and because in-stream biological activity likely contributes disproportionately to whole-river ecosystem function (Wollheim et al., 2022). However, current understanding of in-stream processing is mostly extrapolated from tracer-addition experiments or intensive process monitoring in small, headwater streams (Ensign and Doyle, 2006; Mulholland et al., 2008). Large streams and rivers are subject to a range of complex interactions between hydrodynamics, biological and anthropogenic activities that may limit the applicability of extrapolation from headwater measurements (Bernal et al., 2019). Moreover, owing to the practical challenges of making direct process measurements in large, deep non-wadeable rivers, there is a shortage of data on whole-stream NO_3^- biochemical cycling and its constituent pathways (e.g., assimilation, denitrification, mineralization and nitrification).

Fostered by sensor technology development, high-frequency measurements are increasingly being used to infer in-stream NO_3^- retention and release in large streams and rivers (Rode et al., 2016b). Biochemical process-related information can be directly extracted from NO_3^- timeseries (Burns et al., 2019; Heffernan and Cohen, 2010). However, inferences based purely on high-frequency data are often conducted under well constrained conditions, e.g., a steady-state upstream boundary (Hensley and Cohen, 2016; Yang et al., 2019). While the more adaptive two-station approach allows a dynamic upstream boundary, the inference accuracy is still largely subject to influences of hydraulic transformation (e.g., dispersion Hensley and Cohen, (2016)) and dilution/enrichment from lateral inflow along the reach between upstream and downstream stations (Zhang et al., 2022). Consequently, in-stream process quantifications remain uncertain when extrapolating to various hydro-morphological river conditions outside the monitored reaches. As a result, while continuous high-frequency monitoring has been deployed for multiple years across river sizes and geomorphological conditions (Arndt et al., 2022; Bieroza et al., 2023; Rode et al., 2016b), inferences of in-stream processes using such invaluable long-term data, is often obscure due to dynamic flow conditions and their complex convolutions with biological activity (Hensley and Cohen, 2016; Payn et al., 2017). This complexity has hindered multi-year continuous investigations of in-stream NO_3^- retention, and the responses of in-stream processes to the changing climate, such as the severe droughts in Europe over last five years.

Conventional two-station inferences of in-stream NO_3^- biogeochemical retention along the reach were based on load ($Q \times NO_3^- - N$) differences between the upstream and downstream stations. However, purely using the monitored high-frequency data is challenging to estimate lateral inflows and transport time lags, and their inferences on the calculation require specific justifications (Jarvie et al., 2018; Zhang et al., 2022). Alternatively, high-frequency discharge

(Q) and solute dataset are increasingly used to calibrate river modeling approaches, which normally include both hydraulic transport (advective and dispersive) and biogeochemical retention terms in their master equation of mass balance (Hensley and Cohen, 2016; Huang et al., 2022). However, the simulations of biological processes are often challenged by complex hydraulic-biological convolutions and model parameterization (Rode et al., 2007). To benefit from the complementary data analysis and modelling, here we propose an innovative data-model fusion framework for in-stream process inferences in large streams and rivers. The framework is mainly based on the two-station high-frequency monitoring, but untangling impacts of hydraulic transformations along the reach using the advanced features of the WASP8 water and tracer simulations (Ambrose and Wool, 2017; Knightes et al., 2019). Such methodological improvements are necessary to study the nitrate uptake dynamics under varying climatic and flow conditions.

Here we illustrated the analysis using six years of data from a 27.4 km 6th order reach of the lower Bode River, central Germany. The objectives of this study were: (1) to estimate continuous in-stream NO_3^- overall retention (net uptake/release) over the normal (2015-2017) and drought (2018-2020) years based on the fusion of high-frequency data analysis and modeling; (2) to investigate responses of the in-stream processes to the droughts from sub-daily to inter-annual scales; and (3) to unravel potential environmental factors that control the in-stream processes and their pattern shifts under the drought disturbances.

2 Method and Materials

2.1 Study site and long-term high-frequency monitoring

The Bode River, ca. 169 km long with a watershed area of 3270 km^2, originates in the Harz Mountain area, central Germany. The studied 27.4 km reach of the lower Bode River (6th order) is surrounded by intensive lowland arable land (Figure 1a). Between the study period 2015-2020, multi-parameter high-frequency monitoring equipment was deployed at two stations: the upstream station Groß Germersleben (GGL) and the downstream station Staßfurt (STF). The river reach mostly exhibits rectangular or trapezoidal cross-sections, due to artificial modifications in the 1970s for the purpose of agricultural activities. There are also three overflow weirs installed along the reach. The riverbed substrate consists of mostly sand and small gravel, with an average width and slope of 20 m and 0.4 ‰, respectively. Patchy bankside deciduous trees partially shade the riparian margins during summer, while the relatively open canopy allows high irradiance at the river surface and development of phytoplankton and benthic algae (Huang et al., 2022).

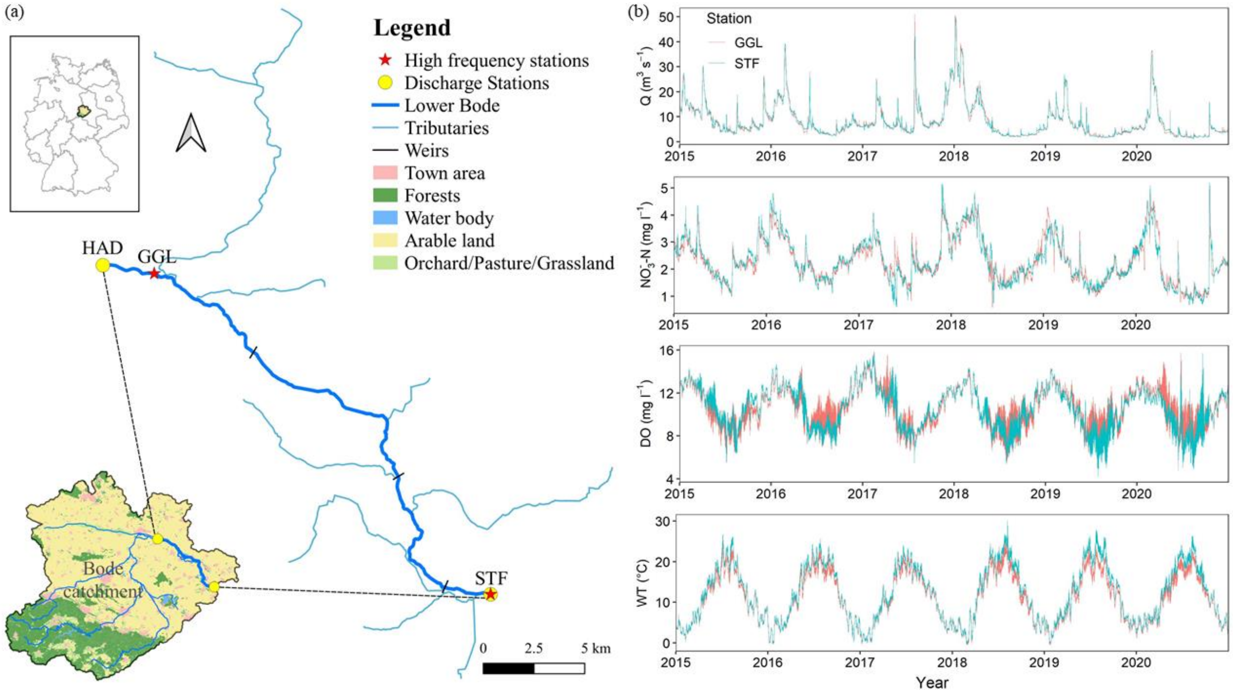

Figure 1. (a) The Lower Bode river reach and the multi-parameter high-frequency monitoring scheme. (b) 15-min measurements of discharge (Q), $NO_3^- - N$ concentrations, dissolved oxygen (DO) and water temperature (WT) at the upper Groß Germersleben (GGL) and lower Staßfurt (STF) stations.

At each station, YSI 610 sensors (Yellow Springs, US) measured dissolved oxygen (DO), pH, water temperature (WT), and electric conductivity (EC) at 15-min intervals. ProPS-UV sensors (TriOS GmbH, Germany) measured spectral absorbance at 254 nm (SAC, as a proxy of dissolved organic carbon) and Nitrate-N ($NO_3^- - N$, precision of 0.03 ±2% mgl^{-1}) concentrations, also at 15-min intervals. More details about sensor accuracy and maintenance were described in Rode et al. (2016a). Hourly data on photosynthetically active radiation (PAR) were collected at an eddy-covariance flux tower at Wulferstedt station (15.6 km north-west of GGL). Discharge (Q) data at 15-min intervals were obtained from the Saxony-Anhalt water authority (Water Service data portal https://gld.lhw-sachsen-anhalt.de/, accessed 4/27/2023) at station Hadmersleben (HAD, 2.7 km upstream of GGL without significant lateral inflows) and station STF (Figure 1a). There are eight small tributaries along the study reach; however, total tributary inputs contributed less than 2% of total Q over 2015-2020 as simulated by the catchment mHM-Nitrate model (Zhou, et. al., 2022).

The study region has experienced dramatically changing climatic conditions, especially severe summer droughts since 2018 (Bakke et al., 2020). Annual average Q at STF decreased from 9.50 m^3s^{-1} during the "normal" years (2015-2017) to 7.21 m^3s^{-1} during the "drought" years (2018-2020) (Figure 1b). Comparing normal- and drought-year summers (Jun-August), average Q decreased from 6.58 to 2.75 m^3s^{-1}, average $NO_3^- - N$ concentration decreased from 1.79 to 1.39 mgl^{-1}, and average WT increased from 20.1 to 21.6 ℃.

2.2 Two-station inferences of NO_3^- retention based on the fusion of high frequency data monitoring and the WASP water and tracer simulations

The WASP model (version 8.32) has been developed by the United States Environmental Protection Agency and has been applied to different surface water systems (Wool et al., 2020). The model allows users to flexibly define and arrange control volumes (i.e., fully mixed finite segments), and resolves the mass balance over each control volume, considering material exchanges via advective and dispersive transports. WASP further distinguishes free-flowing, ponded and backwater/tidal influenced segments in a stream network, and solves them using equations of kinematic wave, weir overflow and dynamic flow, respectively (Ambrose and Wool, 2017). The tracer module implemented in WASP8 is a dummy sub-model for substances with no kinetic interactions.

In this study, we conducted 15-min interval, one-dimensional WASP8 simulations of water and tracer (i.e., conservative $NO_3^- - N$) transport in the study reach. We upgraded a prior WASP model setup in the study reach by Huang et al. (2022), with 31 segments defined as free-flowing reaches and 3 segments as ponded reaches at the locations of the weirs (**Figure 1a**). Discharge at station HAD was used as the upstream flow inputs, and the measured $NO_3^- - N$ concentrations at GGL were taken as the tracer inputs. Inputs of flow and tracer loads from the tributaries were simulated from a catchment mechanistic model mHM-Nitrate (Yang et al., 2018; Yang and Rode, 2020) (see detailed model simulations in the Bode catchment in Zhou et al. (2022)). Using the WASP hydrodynamic simulations, the upstream tracing signals of conservative $NO_3^- - N$ concentration (N_{trck}) were transported to the downstream station STF. Thus, differences between the tracked loading (L_{trck}) predicted by the conservative WASP modeling and the observed loading (L_{obs}) at STF were taken as retention along the river reach. Areal retention rates ($U_T, mgNm^{-2}$ per time step) and efficiencies (E_{UT}, %) can be further obtained based on this data-model fusion inferences:

$$U_T = \frac{L_{trck} - L_{obs}}{A} = \frac{(N_{trck} - N_{obs}) \times Q_{STF}}{A} \tag{1}$$

$$E_{UT} = \frac{L_{trck} - L_{obs}}{L_{trck}} \times 100 \tag{2}$$

where A denotes the total river benthic area (27400×20 m^2). Note that we used observed discharge at STF (Q_{STF}) for L_{trck} to further reduce model uncertainty leveraged from hydraulic simulations (see Section 3). Therefore, U_T represents overall NO_3^- net uptake or net release (with positive and negative values, respectively), and E_{UT} was only analyzed in periods exhibiting net uptake (U_T>0).

2.3 Calculations of stream metabolism and in-stream autotrophic NO_3^- assimilation

Estimates of whole-stream metabolisms (i.e., gross primary production - GPP and ecosystem respiration - ER) were calculated based on the 15-min DO measurements. The hydraulic characteristics at STF were heavily impacted by impoundment effects due to bridge piers and submerged macrophytes, and this hindered the calculations of stream metabolism at STF. Therefore, we applied the single-station method (Odum, 1956) using the data at the upper station GGL, which is representative of the metabolic conditions of the Lower Bode reaches (see detailed justifications in **Text S1** and **Table S1**). Please also refer to Yang et al. (2019) for detailed calculation equations of the single-station approach.

We further estimated $NO_3^- - N$ uptake via autotrophic assimilation based on the whole-stream metabolism at daily time step. Gross assimilations by autotrophs ($U_A, mgNm^{-2}d^{-1}$) can be calculated based on the measured stream metabolism and the stoichiometric C:N ratio:

$$U_A = \frac{r_a \times GPP}{2.286 \times C{:}N} \times 1000 \tag{3}$$

where autotrophic respiratory rate r_a was set as 0.5, assuming one mol of C fixed per mol of O_2 produced, and half of GPP ($gO_2m^{-2}d^{-1}$) becomes net production (Rode et al., 2016a). The molar C:N ratio was 9.4, taken from local biofilm measurements (Kamjunke et al., 2015), and the constant 2.286 (32/14) converts the molar ratios to a mass basis.

2.4 Diel pattern detection and statistical analysis

The 15-min continuous $NO_3^- - N$ retention timeseries allowed assessment of in-stream processes from sub-daily (i.e., the diel patterns) to inter-annual scales. At hourly scale, we specifically investigated diel patterns of net uptake (U_T>0, $mgNm^{-2}h^{-1}$). Dates for this diel pattern analysis were detected sequentially according to (1) U_T>0 for all 24 hours, (2) minimal diel variations in Q (i.e., <50th quantile of coefficient of variations), and (3) generally low-flow conditions (i.e., daily Q < 25th quantile for each year). The constraints of relative steady Q were set to avoid impacts of flow variations on $NO_3^- - N$ signals.

The *k*-mean clustering method was performed to further classify them into different clusters, using the "*stat*" R package (R core team, 2022). Please refer to **Text S2** for details of the *k*-mean clustering analysis. Moreover, statistical analyses were all performed in R software, including the one-way ANOVA test ("*stats*" package, with assumptions fulfilled when reporting *p* values) and the curve fitting (the GAM-based smooth function "*geom_smooth*" in "*ggplot2*" package).

3 Results

3.1 WASP simulations of discharge and traced NO_3^- dynamics

The WASP discharge simulations performed very well at the downstream station STF (i.e., Kling-Gupta Efficiency of 0.98 and percentage bias of 0.7%, **Figure 2**). This indicates that WASP captured water dynamics well in the lower Bode River, in line with Huang et al. (2022). We noted that discharge discrepancies were slightly greater during the recession and driest periods of the drought years 2018-2020, though they were negligible in terms of the general river water dynamics (**Figure 2a**).

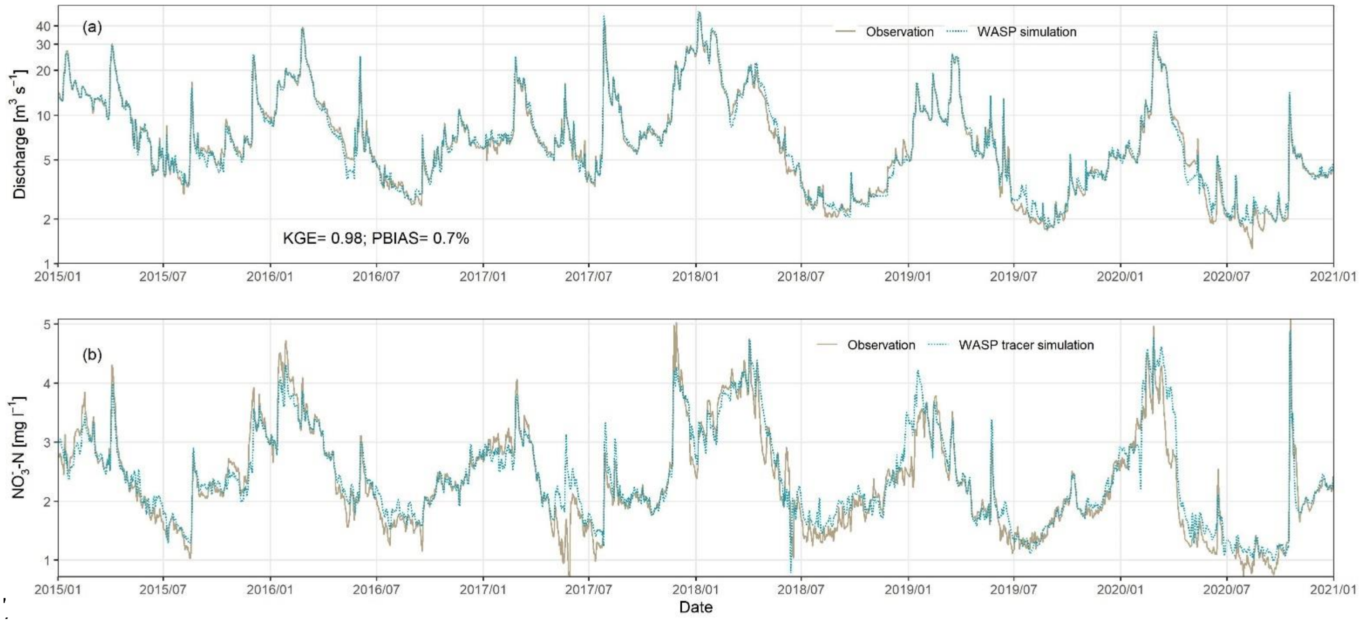

Figure 2. The WASP simulations of discharge (a) and $NO_3^- - N$ tracer concentrations (b) in the reach of the lower Bode River plotted at a daily timestep. Discharge performance criteria KGE and PBIAS represent Kling-Gupta Efficiency and Percentage bias, respectively.

3.2 Daily overall U_T and stream metabolisms and their seasonal variations in the normal and drought years

Continuous daily retention rates U_T were estimated from the data-model fusion from 2015 to 2020 (**Figure 3a**). U_T mostly ranged between -337.8 and 419.4 $mgNm^{-2}d^{-1}$ (i.e., 5% and 95% quantiles, respectively), while the values varied with season and across years. Apart from disturbances of annual high-flows and short-term flow events, U_T exhibited a consistent seasonal pattern in the normal period 2015-2017 (**Figure 3a**, upper panels): (1) winter and early spring seasons exhibited extensive net NO_3^- release (U_T<0), though largely affected by the annual high flows; (2) general net uptake (U_T>0) occurred after the annual high-flow season, with significantly higher retention in May-June than July-September (236.0±224.9 vs 104.7±65.2 $mgNm^{-2}d^{-1}$, among 123 and 230 days, respectively, with Q below the normal-year median value 7.10 m^3s^{-1}; ANOVA test, p<0.001); (3) after October, net NO_3^- release occurred until the next early spring (except for the low winter Q in 2016). For the drought-impacted period 2018-2020 (**Figure 3a**, lower panels), U_T seemed to be still higher during May-June than the later months, while the pattern was heavily disturbed by the annual-high flow recessions and small- to median-size flow events. Moreover, U_T was generally reduced during the annual low-flow seasons (e.g., 47.9±57.2 $mgNm^{-2}d^{-1}$ in July-September, significantly lower than that of the normal years; ANOVA test, p<0.001), and the late-autumn net release during the drought years was not as consistently present as it was during the normal years. The uptake efficiency E_{UT} was higher during the drought than in normal years (10.8±8.1% vs 8.6±9.5%, respectively), and the drought years exhibited prolonged periods with higher E_{UT} (e.g., around 25%, **Figure S1a**).

Figure 3. (a) Daily total retention rate U_T in each year based on the model-data fusion framework, and monthly counts of the four clusters of diel patterns. (b) Daily ratios of whole-stream gross primary production and respiration (i.e., P/R ratio) in the normal (2015-2017) and the drought (2018-2020) years. Note that, for subplot (b), P/R ratios on dates exhibiting diel patterns are highlighted with the same cluster colors as in subplot (a).

Such varying seasonal patterns between the normal and drought years were also observed in the whole-stream metabolic characteristics (**Figures 3b** and **S2**). In spring seasons, the ratio of GPP to ER (P/R) was >1, indicating autotroph-dominated system. This occurred in both the normal and drought years (**Figure 3b**), though in the former it was likely driven by relatively high levels of GPP, while in the latter by relatively low ER (**Figure S2**). During the summer seasons, the P/R ratios varied largely among the normal years, often with similar levels of GPP but more variable ER (**Figure S2**). In contrast, the ratios were more consistent and relatively high in the drought years (0.77±0.20). In autumn and winter, P/R ratios were extensively less than 1, indicating a heterotroph-dominated system for both normal and drought years. Comparatively, the drought years exhibited higher P/R ratios (**Figure 3b**) primarily induced by the significantly lower ERs (i.e., 2.85±1.04 vs 3.65±2.27 $gO_2m^{-2}d^{-1}$ over October-February of the drought and normal years, respectively; ANOVA test, p<0.001, **Figure S2**). The GPP-informed autotrophic NO_3^- uptake (U_A) maintained similar in the normal and drought years (i.e., 47.92±42.76 vs 51.04±42.38 $mgNm^{-2}d^{-1}$, respectively, **Figure S1a**), while its proportions to U_T were more consistently >1 during July-October of the drought years (calculated among dates with U_T>0 and below-median Q, **Figure S1b**).

3.3 Diel patterns of net $NO_3^- - N$ uptake and their predominance under the normal and drought years

The high-frequency data-model fusion inference provided the unique opportunity to investigate sub-daily patterns of $NO_3^- - N$ uptake and their variations under different hydrological conditions. Quantifiable diurnal variation in U_T was detected in a total of 178 days (90 and 88 days in the normal and drought years, respectively), and could be further grouped into four distinct clusters (**Figures 4 and 3,** and detailed results of the *k*-mean clustering in **Figure S3**). Clusters C1 and C2 exhibited increased uptake during the daytime hours, with the diel maxima occur after and before 12:00, respectively (**Figure 4a and b**); Clusters C3 and C4 exhibited decreased uptake during the daytime hours, with the diel minima occur around 12:00 for the former (**Figure 4c**) while the latter exhibited more noteworthy decreases before noon and delayed diel minima (**Figure 4d**). Meanwhile, the seasonal occurrence of the four clusters likely changed between the normal and drought years (the upper and lower panels of **Figure 3a**, respectively). Specifically, in the normal years, C1 and C2 mostly occurred before August, while C3 and C4 dominated the late summer and autumn seasons; in contrast, during drought years C1 and C2 patterns persisted into the late summer and autumn (accounting for 67% of total days detected in the drought years, compared to that of 38% in the normal years), and also more evenly distributed across summer-autumn seasons. The four diel patterns did not show substantial differences between normal and drought years, with the exception of the C1 cluster that exhibited more delayed diel maxima in the normal years than the drought years, (**Figure 4**, upper panels). However, the absolute uptake rates were significantly lower under the drought conditions, except for the C3 cluster even though there existed extraordinarily high uptake days in 2017 (**Figure 4**, lower panels).

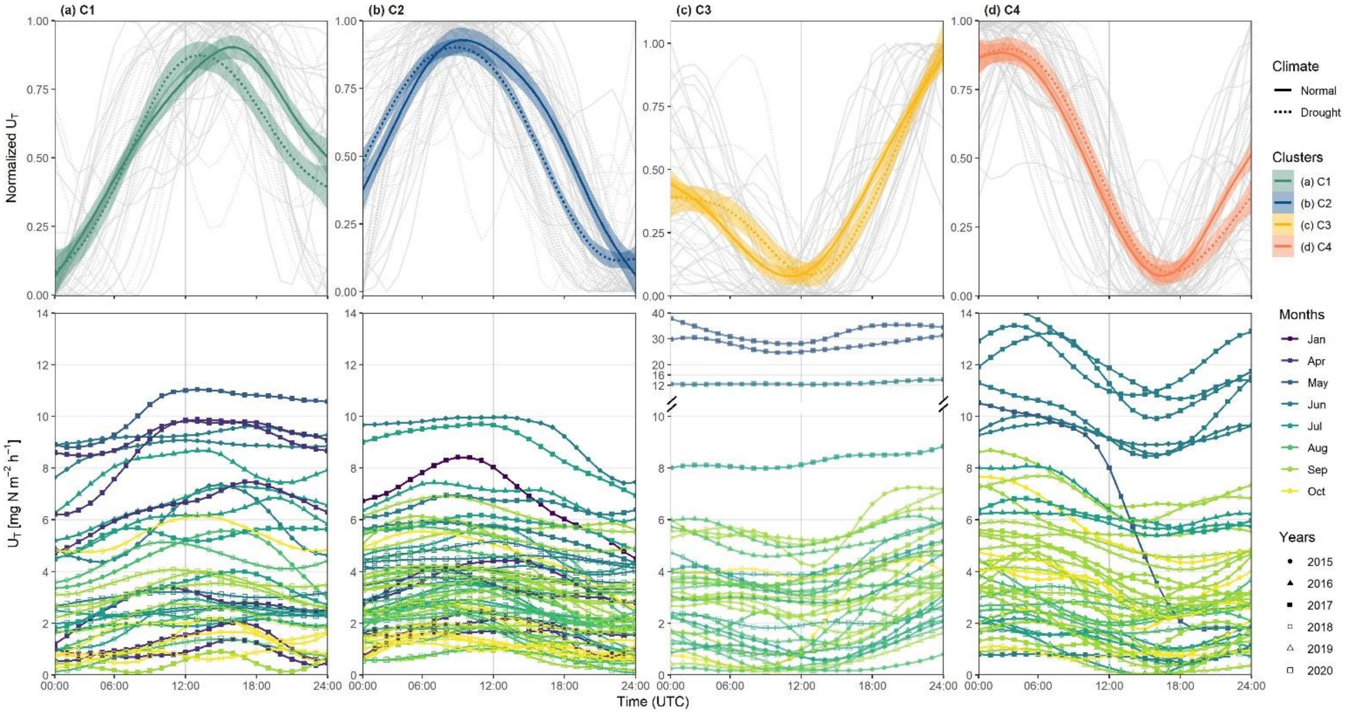

Figure 4. The four types of U_T diel patterns clustered among the detected 178 days and the corresponding hourly variations of retention rates (upper and lower panels, respectively). Note that the *k*-mean clustering was performed based on the max-min normalized U_T values.

4 Discussion

4.1 Continuous inferences of $NO_3^- - N$ retention in complex rivers enabled by a novel high-frequency data-model fusion framework

Using a novel data-model fusion framework, we derived continuous estimates of high-frequency $NO_3^- - N$ retention over six years in the 6th order reach of the lower Bode River. To our knowledge, this is among the first time that such in-stream inferences have been made in a large stream or river with complex flow dynamics as well as across different hydrological conditions. Importantly, the model-data fusion framework provided reasonable estimates of in-stream $NO_3^- - N$ retention in the well-studied lower Bode region, as cross validated by previous studies using different methodologies. For example, previous work (Zhang et al., 2022) using the conventional two-station method reported a similar range and seasonal variations in net $NO_3^- -$

N retention and release (-205 and 381 $mgNm^{-2}d^{-1}$ as for 5th and 95th quantiles, respectively, with consistently higher values in campaigns during May-June than July-September). Huang et al. (2022) applied the WASP biogeochemical modeling in the same lower Bode River reach and calibrated model parameters using the high-frequency data (including only the first drought year 2018). They also obtained generally similar levels of net $NO_3^- - N$ uptake, and similar seasonal patterns (Huang et al., 2022).

Our estimates of in-stream retention rate and retention efficiency were also well in line with wider literature ranges (Alexander et al., 2009; Ensign and Doyle, 2006; Miller et al., 2016; Mulholland et al., 2008; Seitzinger et al., 2002). Ensign and Doyle (2006) reported the interquartile range of 9.1 and 376.7 $mgNm^{-2}d^{-1}$ based on14 nutrient-addition/isotope-tracer experiments conducted in 4th order streams. This fits well with our estimated range of the NO_3^- uptake (**Figure 3a**), which is also similar to the headwater measurements from the pioneering LINX II project (Hall Jr. et al., 2009). Heffernan and Cohen (2010) deployed a high-frequency monitoring in a Florida spring-fed river and revealed that U_T is two times higher in spring than in fall seasons, though the reported magnitude was relatively high due to high denitrification rates in subtropical rivers (Heffernan et al., 2010). Using E_{UT} as a more cross-comparable uptake metric, Seitzinger et al. (2002) found that individual reaches generally retain <20% of N input, and specifically for 5th- and higher-order reaches, the proportions are mostly <10%. This is well in line with our estimated ranges (e.g., mostly < 20.8% as of the 90% quantile value over the six years).

The high-frequency data-model fusion framework allows assessment of in-stream processes to be extended across temporal and spatial scales, thereby advancing understanding of NO_3^- processes. First, the framework can make use of the increasingly available long-term time series of high-frequency monitoring, being collected as part of routine monitoring by water authorities. Given the logistic convenience and advances of cross-parameter analysis (Rode et al., 2016b; van Geer et al., 2016), these continuous sensor deployments are often co-located with flow gauging stations, allowing assessment of varying and complex flow regimes and their impacts on biogeochemical processes (Bieroza et al., 2023; Oldham et al., 2013). Integrating the robust in-stream hydraulic and conservative tracer modeling facilitates the extraction of biogeochemically induced nutrient signals, even with shifts between advective and dispersive flow dominance and variations in water residence/travel times (Hensley and Cohen, 2016). This, in our view, serves as a step forward in maximizing the multi-benefits of these unique datasets, especially compared to the uses of constraining synthesized in-stream water quality models at a finer temporal resolution (though still informative, see Huang et al., (2022); Khorashadi Zadeh et al., (2019)).

Second, the framework quantifies in-stream NO_3^- retention from sub-daily to inter-annual scales, providing new process understanding (see discussion in Section 4.2) and reference values for specific processes. For instance, the WASP modeling by Huang et al., (2022) also revealed the consistent pattern of net release after late-autumn (i.e., U_T<0), while with more conservative estimates (17.4 $mgNm^{-2}d^{-1}$ compared to our inferences of >100 $mgNm^{-2}d^{-1}$, **Figure 3a**). Given the well-acknowledged poor process understanding (von Schiller et al., 2015) and the simplified model conceptualization, our inferences derived more directly from high-frequency data, can be further used to validate model simulations and improve in-stream process representation in water quality models.

There are several considerations when transferring the framework to a wider context. Firstly, the estimation uncertainty may be large during high-flow seasons and short-term runoff events, primarily induced by contributions from tributaries and lateral subsurface inflows. These lateral inputs are often ungauged and elevated during hydrologically active periods. Particularly for the lower Bode region, the high groundwater concentrations (up to > 10 $mgNl^{-1}$, the authority data portal https://gld.lhw-sachsen-anhalt.de/) in the agricultural landscape might strongly affect riverine concentrations even under small runoff events (as illustrated by the discharge-concentration hystereses in Zhang et al. (2020)). However, we cautiously estimated tributary inputs using the grid-based catchment modeling (Zhou et al., 2022), and found that the lateral loading inputs were marginal, as this was generally a loosing channel (Kunz et al., 2017; Zhang et al., 2022). Moreover, hyporheic exchange might need to be explicitly included in the hydraulic and tracer simulations, where the process is known to be significant and sufficient data are available to constrain it (Gomez-Velez et al., 2015).

4.2 Insights into seasonal patterns of NO_3^- retention and release under the changing climate

Both net NO_3^- uptake (U_T>0) and net NO_3^- release (U_T<0) exhibited substantial seasonality, which also differed between the normal (2015-2017) and drought (2018-2020) years. Moreover, this variation was well supported by the independent calculations of stream metabolic characteristics, which also exhibited strong seasonality (**Figure 3** and **S2**).

Despite the flow-induced uncertainty during the high-flow periods, winter to early-spring seasons showed extensive net NO_3^- release, which was more pronounced in the normal years than the drought years. Meanwhile, the normal-year P/R $\ll$1 and ER remained as high as that in the summer seasons, indicating higher heterotrophic microbiological activity during the normal year. Such net heterotrophy likely also reflects reduced rates of autotrophic activity (due to seasonally lower light availability and water temperature) and promoted remineralization processes (given that riverine dissolved organic carbon (DOC) is abundantly flushed from the catchment and riparian areas). The DOC in anthropogenically affected rivers is likely more labile to the microbial community than in unaffected rivers (Graeber et al., 2012; Stutter et al., 2018). Meanwhile the relatively high water temperature (i.e., interquartile range of 3.4 and 7.9 ℃) may have contributed to higher rates of microbiological transformation of DOC (Lu et al., 2013). However, under sequential droughts, the recalcitrance of DOC could have been increased due to the longer exposure times of terrestrial organic matter to catchment microbiological transformations before being transported (Catalán et al., 2016) and that the enzymatic hydrolysis of the recalcitrant components is limited with increasing temperature (Evans et al., 2005; Freeman et al., 2001). This agrees well with the observed low ERs (**Figure S2**) but with largely maintained DOC concentrations during the drought years (as indicated by the surrogate SAC measurements, although direct DOC quality information was missing). Also, the reduced levels of net NO_3^- release during winter and early-spring seasons may be ascribed to the drought-induced reduction of heterotrophic activity.

The extensive net uptake patterns during the mid-spring to early-autumn warmer seasons are well in line with general literature findings that highlight the significant nutrient "cleansing function" of lotic ecosystems, while the dominant mechanisms could vary largely under different stream and climatic conditions (Heffernan and Cohen, 2010; Jarvie et al., 2018; Jones et al., 2015). The net uptake reached the highest level between mid-spring and early-summer, associated with the promoted and autotrophy-dominated ecosystem activities (the high P/R ratios and increased GPP and ER, **Figures 3** and **S2**). The normal-year overall net uptake was still greater than the autotrophic assimilation, although with increasing amount and proportions for the latter pathway. This indicates that (1) autotrophic assimilation played a dominant role in $NO_3^- - N$ uptake, primarily due to the sufficient light availability during the season before leaf-out (Rode et al., 2016a; Yang et al., 2019) and (2) other uptake pathways via heterotrophic direct assimilation and denitrification were likely substantial in the normal years, given the abundant nutrient and organic matter availability (Kamjunke et al., 2013). In contrast, the drought years exhibited relatively reduced overall net uptake and ER, but a similar level of GPP, together resulting in earlier, more consistent U_A/U_T >1 (**Figure S1b**). This indicates an earlier predominance of autotrophic assimilation, which is also buffered partly by N-release processes (Jarvie et al., 2018). The reduction in other heterotrophic pathways is likely ascribed to the limited allochthonous labile DOC during the droughts, given the synchronous changes between ER and $NO_3^- - N$ uptake (Stutter et al., 2018; Sunjidmaa et al., 2022).

Nevertheless, autochthonous DOC from antecedent primary production may have provided an important energy source for heterotrophs in the lower Bode River during the driest summer and autumn seasons, in accordance with reduced catchment hydrological connectivity. This is evidenced by the increasingly buffered autotrophic assimilation ($U_A/U_T \gg 1$) and generally decreased net NO_3^- uptake, both of which exhibited higher degrees of changes in the drought years. This is supported by DOC measurements across the Bode River network by Kamjunke et al. (2013), that the September samples from the lower Bode River exhibited better DOC quality (i.e., lower molecular weights and lower humic content) than the headwater samples. Also, Dupas et al. (2017) demonstrated that the Bode lowland aquatic systems likely acted as a DOC source. There is a pressing and strategic need for better mechanistic understanding of the responses of river ecosystems to climate variability. Our results suggest that reduced inputs of allochthonous labile DOC during prolonged droughts may have resulted in shifts to greater and more sustained utilization of autochthonous DOC by microbes, corresponding with reductions in both net NO_3^- retention and net release.

4.3 Insights into diel patterns of NO_3^- retention under the changing climate

The high-frequency data-model fusion framework also allowed in-depth investigations of diel patterns of $NO_3^- - N$ uptake. Here we identified four distinct clusters of diel patterns, as well as their seasonal distributions, revealing shifts in dominant NO_3^- retention processes under normal and drought conditions. We can speculate as to some of the underlying mechanisms potentially responsible for generating these patterns.

Cluster C1 represented a typical autotrophic assimilation induced diel pattern, which is correlated with the diurnal variations of GPP and related environmental factors (e.g., radiation, temperature and DO; **Figures 4a, S4a and S5**). Interestingly, the diel uptake maxima were delayed relative to those of GPP, indicating physiological time lags between $NO_3^- - N$ uptake and photosynthesis. This is potentially due to photosynthesis providing additional energy to further reduce NO_3^- for assimilation and biosynthesis (Mulholland et al., 2006). The observed time-lag differences between normal and drought years are in line with the spring-fall differences reported by Heffernan and Cohen (2010), which may be related to seasonal differences of such energetic costs.

Cluster C2 also largely represented the dominance of autotrophic assimilation, given the extensive positive correlations with GPP-related factors (**Figure S4**) and their well-fitted falling limbs after 12:00 (**Figure S5b**). Besides, as a concatenation of Cluster 1 and Clusters 3/4, NO_3^- autotrophic assimilation in the afternoon might be buffered to a greater extent by release processes, resulting in apparently earlier net uptake maxima. These diurnally earlier NO_3^- uptake peaks are also reported in high-frequency NO_3^- data analysis, with complex, often unclear mechanisms (Aubert and Breuer, 2016; Greiwe et al., 2021; Heffernan and Cohen, 2010). Here we observed that (1) this pattern occurred mostly after high-flow recessions in the normal years (**Figure 3a**), which is coincidently presented by Aubert and Breuer (2016) via data mining of NO_3^- timeseries; (2) the high correlations with SAC in drought years at the diurnally normalized scale (**Figures S4 and S5b**). This indicates a crucial role of DOC availability, particularly its quality as aforementioned, in shaping (either promoting or constraining) the diel pattern of NO_3^- uptake.

Clusters C3 and C4 revealed less-explored diel patterns with diel minima uptake during the daytime. For C3, diel minima occurred nearly at mid-day hours, the timing of GPP and temperature maxima (**Figure S5c**); meanwhile, the NO_3^- uptake (U_T and the U_A pathway) and metabolisms (GPP, ER and their ratios) were similar to Clusters C1 and C2, indicating high daytime photosynthesis. The exact mechanisms would need further specific investigations, while possible explanations could be: (1) this pattern occurred mostly during late summer and autumn, when diel variations of denitrification rates govern the net NO_3^- uptake patterns; (2) redox controls (linked to high daytime O_2 production by photosynthesis) will likely suppress denitrification, resulting in diel minima during daytime hours. The C4 pattern was highly comparable with C3 (see **Figure 4c-d**, and the clustering results in **Figure S3**), while likely exhibited higher rates of heterotrophic-related uptake like denitrification (linked to lower P/R ratios **Figure 3b**, and significantly positive correlations with SAC **Figure S4**).

In addition to specific mechanistic understanding of the four cluster types, their seasonal distributions and changes between normal and drought years (**Figure 3a**, bar-plots), also reveal shifts in river ecosystem function. In the normal years, the autotrophy-characterized C1 and C2 patters mostly occur during earlier seasons, which are then followed by a shift to heterotrophy-dominated C3 and C4 patterns during later summer-autumn low-flow periods. However, the sequential droughts have shifted this seasonal distribution to greater persistence of C1 and C2 across seasons, extending the window of autotrophic dominance into the late summer and autumn. Such varying seasonal distributions of diel patterns are likely linked to the drought-induced changes in catchment and stream environmental factors and their contrasting impacts on in-stream NO_3^- biogeochemical processes. This also corresponds with the seasonal insights derived based on the daily timeseries (Section 4.2) that showed a shift to greater persistence of net autotrophy during the drought years.

5 Conclusion

This study proposed a data-model fusion framework that enables continuous inferences of in-stream NO_3^- biogeochemical processes in large streams and rivers, overcoming major methodological constraints of using high-frequency monitoring data under variable flow and climatic conditions. Long-term high-frequency estimates in the 6th-order lower Bode River further revealed new insights into NO_3^- dynamics in relation to river ecosystem function, from sub-daily to seasonal scales and under a range of flow conditions. These estimates of net in-stream retention and release, derived closely from direct *in-situ* measurements, provide useful reference values, e.g., for model validation or process conceptualization. Also, identifying and deconvoluting shifts in river ecosystem function (between autotrophy- and heterotrophy-dominance) are of key importance for understanding the impacts of climate change on water quality, ecological status and river function.

This high-frequency data-model fusion method can be applied across sites and scales, and provides an opportunity for scientists and river managers to capitalize on the emergent wave of high-frequency water-quality monitoring. The method can also be extended from small-streams under dynamic flow conditions, to river network scale applications coupled with catchment models. Moreover, the method can complement high-frequency monitoring for cost-effective evaluation of the effectiveness of management practices and river-restoration projects.

Acknowledgement

Xiaoqiang Yang and Xiaolin Zhang contributed equality to this work. Xiaolin Zhang is funded by the Chinese Scholarship Council (CSC). We thank Uwe Kiwel for his technical support during the field work. The authors thank Jingshui Huang for sharing the WASP7 set-up. The authors also thank the Federal Agency for Cartography and Geodesy (BKG) and the State Agency for Flood Protection and Water Management of Saxony Anhalt (LHW) for all data support.

References

Alexander, R.B., Böhlke, J.K., Boyer, E.W., David, M.B., Harvey, J.W., Mulholland, P.J., Seitzinger, S.P., Tobias, C.R., Tonitto, C., Wollheim, W.M., 2009. Dynamic modeling of nitrogen losses in river networks unravels the coupled effects of hydrological and biogeochemical processes. Biogeochemistry 93, 91–116. https://doi.org/10.1007/s10533-008-9274-8

Ambrose, R.B., Wool, T., 2017. WASP8 Stream Transport - Model Theory and User's Guide. U.S. Environmental Protection Agency, Office of Research and Development, Washington.

Arndt, J., Kirchner, J.S., Jewell, K.S., Schluesener, M.P., Wick, A., Ternes, T.A., Duester, L., 2022. Making waves: Time for chemical surface water quality monitoring to catch up with its technical potential. Water Res. 213, 118168. https://doi.org/10.1016/j.watres.2022.118168

Aubert, A.H., Breuer, L., 2016. New Seasonal Shift in In-Stream Diurnal Nitrate Cycles Identified by Mining High-Frequency Data. PLOS ONE 11, e0153138. https://doi.org/10.1371/journal.pone.0153138

Bakke, S.J., Ionita, M., Tallaksen, L.M., 2020. The 2018 northern European hydrological drought and its drivers in a historical perspective. Hydrol. Earth Syst. Sci. 24, 5621–5653. https://doi.org/10.5194/hess-24-5621-2020

Bernal, S., Lupon, A., Wollheim, W.M., Sabater, F., Poblador, S., Martí, E., 2019. Supply, Demand, and In-Stream Retention of Dissolved Organic Carbon and Nitrate During Storms in Mediterranean Forested Headwater Streams. Front. Environ. Sci. 7.

Bieroza, M., Acharya, S., Benisch, J., ter Borg, R.N., Hallberg, L., Negri, C., Pruitt, A., Pucher, M., Saavedra, F., Staniszewska, K., van't Veen, S.G.M., Vincent, A., Winter, C., Basu, N.B., Jarvie, H.P., Kirchner, J.W., 2023. Advances in Catchment Science, Hydrochemistry, and Aquatic Ecology Enabled by High-Frequency Water Quality Measurements. Environ. Sci. Technol. 57, 4701–4719. https://doi.org/10.1021/acs.est.2c07798

Burns, D.A., Pellerin, B.A., Miller, M.P., Capel, P.D., Tesoriero, A.J., Duncan, J.M., 2019. Monitoring the riverine pulse: Applying high-frequency nitrate data to advance integrative understanding of biogeochemical and hydrological processes. WIREs Water 6, e1348. https://doi.org/10.1002/wat2.1348

Catalán, N., Marcé, R., Kothawala, D.N., Tranvik, L.J., 2016. Organic carbon decomposition rates controlled by water retention time across inland waters. Nat. Geosci. 9, 501–504. https://doi.org/10.1038/ngeo2720

Costa, D., Sutter, C., Shepherd, A., Jarvie, H., Wilson, H., Elliott, J., Liu, J., Macrae, M., 2022. Impact of climate change on catchment nutrient dynamics: insights from around the world. Environ. Rev. https://doi.org/10.1139/er-2021-0109

Dupas, R., Musolff, A., Jawitz, J.W., Rao, P.S.C., Jäger, C.G., Fleckenstein, J.H., Rode, M., Borchardt, D., 2017. Carbon and nutrient export regimes from headwater catchments to downstream reaches. Biogeosciences 14, 4391–4407. https://doi.org/10.5194/bg-14-4391-2017

EEA, 2021. Drivers of and pressures arising from selected key water management challenges — A European overview (Publication No. 09/2021). European Environment Agency, Copenhagen, Denmark.

Ensign, S.H., Doyle, M.W., 2006. Nutrient spiraling in streams and river networks. J. Geophys. Res. Biogeosciences 111. https://doi.org/10.1029/2005JG000114

Evans, C.D., Monteith, D.T., Cooper, D.M., 2005. Long-term increases in surface water dissolved organic carbon: Observations, possible causes and environmental impacts. Environ. Pollut., Recovery from acidificationin the UK: Evidence from 15 years of acid waters monitoring 137, 55–71. https://doi.org/10.1016/j.envpol.2004.12.031

Freeman, C., Evans, C.D., Monteith, D.T., Reynolds, B., Fenner, N., 2001. Export of organic carbon from peat soils. Nature 412, 785–785. https://doi.org/10.1038/35090628

Gomez-Velez, J.D., Harvey, J.W., Cardenas, M.B., Kiel, B., 2015. Denitrification in the Mississippi River network controlled by flow through river bedforms. Nat. Geosci. 8, 941. https://doi.org/10.1038/ngeo2567

Graeber, D., Gelbrecht, J., Pusch, M.T., Anlanger, C., von Schiller, D., 2012. Agriculture has changed the amount and composition of dissolved organic matter in Central European headwater streams. Sci. Total Environ. 438, 435–446. https://doi.org/10.1016/j.scitotenv.2012.08.087

Greiwe, J., Weiler, M., Lange, J., 2021. Diel patterns in stream nitrate concentration produced by in-stream processes. Biogeosciences 18, 4705–4715. https://doi.org/10.5194/bg-18-4705-2021

Hall Jr., R.O., Tank, J.L., Sobota, D.J., Mulholland, P.J., O'Brien, J.M., Dodds, W.K., Webster, J.R., Valett, H.M., Poole, G.C., Peterson, B.J., Meyer, J.L., McDowell, W.H., Johnson, S.L., Hamilton, S.K., Grimm, N.B., Gregory, S.V., Dahm, C.N., Cooper, L.W., Ashkenas, L.R., Thomas, S.M., Sheibley, R.W., Potter, J.D., Niederlehner, B.R., Johnson, L.T., Helton, A.M., Crenshaw, C.M., Burgin, A.J., Bernot, M.J., Beaulieu, J.J., Arangob, C.P., 2009. Nitrate removal in stream ecosystems measured by 15N addition experiments: Total uptake. Limnol. Oceanogr. 54, 653–665. https://doi.org/10.4319/lo.2009.54.3.0653

Heffernan, J.B., Cohen, M.J., 2010. Direct and indirect coupling of primary production and diel nitrate dynamics in a subtropical spring-fed river. Limnol. Oceanogr. 55, 677–688. https://doi.org/10.4319/lo.2010.55.2.0677

Heffernan, J.B., Cohen, M.J., Frazer, T.K., Thomas, R.G., Rayfield, T.J., Gulley, J., Martin, J.B., Delfino, J.J., Graham, W.D., 2010. Hydrologic and biotic influences on nitrate removal in a subtropical spring-fed river. Limnol. Oceanogr. 55, 249–263. https://doi.org/10.4319/lo.2010.55.1.0249

Hensley, R.T., Cohen, M.J., 2016. On the emergence of diel solute signals in flowing waters. Water Resour. Res. 52, 759–772. https://doi.org/10.1002/2015WR017895

Huang, J., Borchardt, D., Rode, M., 2022. How do inorganic nitrogen processing pathways change quantitatively at daily, seasonal and multi-annual scales in a large agricultural stream? Hydrol. Earth Syst. Sci. 1–23. https://doi.org/10.5194/hess-2021-615

Jäger, C.G., Hagemann, J., Borchardt, D., 2017. Can nutrient pathways and biotic interactions control eutrophication in riverine ecosystems? Evidence from a model driven mesocosm experiment. Water Res. 115, 162–171. https://doi.org/10.1016/j.watres.2017.02.062

Jarvie, H.P., Sharpley, A.N., Kresse, T., Hays, P.D., Williams, R.J., King, S.M., Berry, L.G., 2018. Coupling High-Frequency Stream Metabolism and Nutrient Monitoring to Explore Biogeochemical Controls on Downstream Nitrate Delivery. Environ. Sci. Technol. 52, 13708–13717. https://doi.org/10.1021/acs.est.8b03074

Jones, C.N., Scott, D.T., Guth, C., Hester, E.T., Hession, W.C., 2015. Seasonal Variation in Floodplain Biogeochemical Processing in a Restored Headwater Stream. Environ. Sci. Technol. 49, 13190–13198. https://doi.org/10.1021/acs.est.5b02426

Kamjunke, N., Büttner, O., Jäger, C.G., Marcus, H., von Tümpling, W., Halbedel, S., Norf, H., Brauns, M., Baborowski, M., Wild, R., Borchardt, D., Weitere, M., 2013. Biogeochemical patterns in a river network along a land use gradient. Environ. Monit. Assess. 185, 9221–9236. https://doi.org/10.1007/s10661-013-3247-7

Kamjunke, N., Mages, M., Büttner, O., Marcus, H., Weitere, M., 2015. Relationship between the elemental composition of stream biofilms and water chemistry—a catchment approach. Environ. Monit. Assess. 187, 432. https://doi.org/10.1007/s10661-015-4664-6

Khorashadi Zadeh, F., Nossent, J., Woldegiorgis, B.T., Bauwens, W., van Griensven, A., 2019. Impact of measurement error and limited data frequency on parameter estimation and uncertainty quantification. Environ. Model. Softw. 118, 35–47. https://doi.org/10.1016/j.envsoft.2019.03.022

Knightes, C.D., Ambrose, R.B., Avant, B., Han, Y., Acrey, B., Bouchard, D.C., Zepp, R., Wool, T., 2019. Modeling framework for simulating concentrations of solute chemicals, nanoparticles, and solids in surface waters and sediments: WASP8 Advanced Toxicant Module. Environ. Model. Softw. 111, 444–458. https://doi.org/10.1016/j.envsoft.2018.10.012

Kunz, J.V., Annable, M.D., Rao, S., Rode, M., Borchardt, D., 2017. Hyporheic Passive Flux Meters Reveal Inverse Vertical Zonation and High Seasonality of Nitrogen Processing in an Anthropogenically Modified Stream (Holtemme, Germany). Water Resour. Res. 53, 10155–10172. https://doi.org/10.1002/2017WR020709

Lu, Y., Bauer, J.E., Canuel, E.A., Yamashita, Y., Chambers, R.M., Jaffé, R., 2013. Photochemical and microbial alteration of dissolved organic matter in temperate headwater streams associated with different land use. J. Geophys. Res. Biogeosciences 118, 566–580. https://doi.org/10.1002/jgrg.20048

Miller, M.P., Tesoriero, A.J., Capel, P.D., Pellerin, B.A., Hyer, K.E., Burns, D.A., 2016. Quantifying watershed-scale groundwater loading and in-stream fate of nitrate using high-frequency water quality data. Water Resour. Res. 52, 330–347. https://doi.org/10.1002/2015WR017753

Mulholland, P.J., Helton, A.M., Poole, G.C., Hall, R.O., Hamilton, S.K., Peterson, B.J., Tank, J.L., Ashkenas, L.R., Cooper, L.W., Dahm, C.N., Dodds, W.K., Findlay, S.E.G., Gregory, S.V., Grimm, N.B., Johnson, S.L., McDowell, W.H., Meyer, J.L., Valett, H.M., Webster, J.R., Arango, C.P., Beaulieu, J.J., Bernot, M.J., Burgin, A.J., Crenshaw, C.L., Johnson, L.T., Niederlehner, B.R., O’Brien, J.M., Potter, J.D., Sheibley, R.W., Sobota, D.J., Thomas, S.M., 2008. Stream denitrification across biomes and its response to anthropogenic nitrate loading. Nature 452, 202–205. https://doi.org/10.1038/nature06686

Mulholland, P.J., Thomas, S.A., Valett, H.M., Webster, J.R., Beaulieu, J., 2006. Effects of light on NO3− uptake in small forested streams: diurnal and day-to-day variations. J. North Am. Benthol. Soc. 25, 583–595. https://doi.org/10.1899/0887-3593(2006)25[583:EOLONU]2.0.CO;2

Odum, H.T., 1956. Primary Production in Flowing Waters1. Limnol. Oceanogr. 1, 102–117. https://doi.org/10.4319/lo.1956.1.2.0102

Oldham, C.E., Farrow, D.E., Peiffer, S., 2013. A generalized Damköhler number for classifying material processing in hydrological systems. Hydrol. Earth Syst. Sci. 17, 1133–1148. https://doi.org/10.5194/hess-17-1133-2013

Payn, R.A., Hall Jr., R.O., Kennedy, T.A., Poole, G.C., Marshall, L.A., 2017. A coupled metabolic-hydraulic model and calibration scheme for estimating whole-river metabolism during dynamic flow conditions. Limnol. Oceanogr. Methods 15, 847–866. https://doi.org/10.1002/lom3.10204

Reusch, T.B.H., Dierking, J., Andersson, H.C., Bonsdorff, E., Carstensen, J., Casini, M., Czajkowski, M., Hasler, B., Hinsby, K., Hyytiäinen, K., Johannesson, K., Jomaa, S., Jormalainen, V., Kuosa, H., Kurland, S., Laikre, L., MacKenzie, B.R., Margonski, P., Melzner, F., Oesterwind, D., Ojaveer, H., Refsgaard, J.C., Sandström, A., Schwarz, G., Tonderski, K., Winder, M., Zandersen, M., 2018. The Baltic Sea as a time machine for the future coastal ocean. Sci. Adv. 4. https://doi.org/10.1126/sciadv.aar8195

Rockström, J., Steffen, W., Noone, K., Persson, Å., Chapin, F.S., Lambin, E.F., Lenton, T.M., Scheffer, M., Folke, C., Schellnhuber, H.J., Nykvist, B., de Wit, C.A., Hughes, T., van der Leeuw, S., Rodhe, H., Sörlin, S., Snyder, P.K., Costanza, R., Svedin, U., Falkenmark, M., Karlberg, L., Corell, R.W., Fabry, V.J., Hansen, J., Walker, B., Liverman, D., Richardson, K., Crutzen, P., Foley, J.A., 2009. A safe operating space for humanity. Nature 461, 472–475. https://doi.org/10.1038/461472a

Rode, M., Halbedel née Angelstein, S., Anis, M.R., Borchardt, D., Weitere, M., 2016a. Continuous In-Stream Assimilatory Nitrate Uptake from High-Frequency Sensor Measurements. Environ. Sci. Technol. 50, 5685–5694. https://doi.org/10.1021/acs.est.6b00943

Rode, M., Suhr, U., Wriedt, G., 2007. Multi-objective calibration of a river water quality model—Information content of calibration data. Ecol. Model. 204, 129–142. https://doi.org/10.1016/j.ecolmodel.2006.12.037

Rode, M., Wade, A.J., Cohen, M.J., Hensley, R.T., Bowes, M.J., Kirchner, J.W., Arhonditsis, G.B., Jordan, P., Kronvang, B., Halliday, S.J., Skeffington, R.A., Rozemeijer, J.C., Aubert, A.H., Rinke, K., Jomaa, S., 2016b. Sensors in the Stream: The High-Frequency Wave of the Present. Environ. Sci. Technol. 50, 10297–10307. https://doi.org/10.1021/acs.est.6b02155

Seitzinger, S.P., Styles, R.V., Boyer, E.W., Alexander, R.B., Billen, G., Howarth, R.W., Mayer, B., van Breemen, N., 2002. Nitrogen retention in rivers: model development and application to watersheds in the northeastern U.S.A. Biogeochemistry 57, 199–237. https://doi.org/10.1023/A:1015745629794

Stutter, M.I., Graeber, D., Evans, C.D., Wade, A.J., Withers, P.J.A., 2018. Balancing macronutrient stoichiometry to alleviate eutrophication. Sci. Total Environ. 634, 439–447. https://doi.org/10.1016/j.scitotenv.2018.03.298

Sunjidmaa, N., Mendoza-Lera, C., Hille, S., Schmidt, C., Borchardt, D., Graeber, D., 2022. Carbon limitation may override fine-sediment induced alterations of hyporheic nitrogen and phosphorus dynamics. Sci. Total Environ. 837, 155689. https://doi.org/10.1016/j.scitotenv.2022.155689

van Geer, F.C., Kronvang, B., Broers, H.P., 2016. High-resolution monitoring of nutrients in groundwater and surface waters: process understanding, quantification of loads and concentrations, and management applications. Hydrol. Earth Syst. Sci. 20, 3619–3629. https://doi.org/10.5194/hess-20-3619-2016

von Schiller, D., Bernal, S., Sabater, F., Martí, E., 2015. A round-trip ticket: the importance of release processes for in-stream nutrient spiraling. Freshw. Sci. 34, 20–30. https://doi.org/10.1086/679015

Wollheim, W.M., Harms, T.K., Robison, A.L., Koenig, L.E., Helton, A.M., Song, C., Bowden, W.B., Finlay, J.C., 2022. Superlinear scaling of riverine biogeochemical function with watershed size. Nat. Commun. 13, 1230. https://doi.org/10.1038/s41467-022-28630-z

Wool, T., Ambrose, R.B., Martin, J.L., Comer, A., 2020. WASP 8: The next generation in the 50-year evolution of USEPA’s water quality model. Water Basel 12, 1398. https://doi.org/10.3390/W12051398

Yang, X., Jomaa, S., Büttner, O., Rode, M., 2019. Autotrophic nitrate uptake in river networks: A modeling approach using continuous high-frequency data. Water Res. 157, 258–268. https://doi.org/10.1016/j.watres.2019.02.059

Yang, X., Jomaa, S., Zink, M., Fleckenstein, J.H., Borchardt, D., Rode, M., 2018. A new fully distributed model of nitrate transport and removal at catchment scale. Water Resour. Res. 54, 5856–5877. https://doi.org/10.1029/2017WR022380

Yang, X., Rode, M., 2020. A Fully Distributed Catchment Nitrate Model - mHM-Nitrate v2.0. https://doi.org/10.5281/zenodo.3891629

Zhang, X., Yang, X., Hensley, R., Lorke, A., Rode, M., 2022. Disentangling in-stream nitrate uptake pathways based on two-station high-frequency monitoring in high-order streams. Water Resour. Res. Rev.

Zhang, X., Yang, X., Jomaa, S., Rode, M., 2020. Analyzing impacts of seasonality and landscape gradient on event-scale nitrate-discharge dynamics based on nested high-frequency monitoring. J. Hydrol. 591. https://doi.org/10.1016/j.jhydrol.2020.125585

Zhou, X., Jomaa, S., Yang, X., Merz, R., Wang, Y., Rode, M., 2022. Exploring the relations between sequential droughts and stream nitrogen dynamics in central Germany through catchment-scale mechanistic modelling. J. Hydrol. 614, 128615. https://doi.org/10.1016/j.jhydrol.2022.128615